Neuron, Vol. 40, 1147–1160, December 18, 2003, Copyright ©2003 by Cell Press

Retinotopic Map Refinement Requires Spontaneous Retinal Waves during a Brief Critical Period of Development

Todd McLaughlin,[1,3] Christine L. Torborg,[2,3] Marla B. Feller,[2,*] and Dennis D.M. O'Leary[1,*]
[1]Molecular Neurobiology Lab
The Salk Institute
La Jolla, California 92037
[2]Neurobiology Section
Division of Biological Sciences
University of California, San Diego
La Jolla, California 92093

Summary

During retinocollicular map development, spontaneous waves of action potentials spread across the retina, correlating activity among neighboring retinal ganglion cells (RGCs). To address the role of retinal waves in topographic map development, we examined wave dynamics and retinocollicular projections in mice lacking the β2 subunit of the nicotinic acetylcholine receptor. $\beta2^{-/-}$ mice lack waves during the first postnatal week, but RGCs have high levels of uncorrelated firing. By P8, the wild-type retinocollicular projection remodels into a refined map characterized by axons of neighboring RGCs forming focal termination zones (TZs) of overlapping arbors. In contrast, in P8 $\beta2^{-/-}$ mice, neighboring RGC axons form large TZs characterized by broadly distributed arbors. At P8, glutamatergic retinal waves appear in $\beta2^{-/-}$ mice, and later, visually patterned activity appears, but the diffuse TZs fail to remodel. Thus, spontaneous retinal waves that correlate RGC activity are required for retinotopic map remodeling during a brief early critical period.

Introduction

In the adult brain, neural systems exhibit a hierarchy of functional organization that reflects distinct arrangements of axonal connections. This organization is the result of a developmental process during which axons make a series of pathfinding choices and undergo stereotypic branching along their length to reach their targets, within which they establish orderly sets of synaptic connections (Burden et al., 2003). The visual system has been a prominent model of both the functional organizations of sensory systems and the mechanisms that control their development. Two distinct fundamental organizational features of axonal connections in the mammalian visual system are interdigitated regions of eye-specific connections and topographic maps (Reid, 2003).

Eye-specific connections are patterned in a manner that keeps inputs from the two eyes segregated, allowing them to be brought together in selective manners for higher-order processing to generate binocular vision and stereopsis. Topographic maps generate a representation of the visual world in the brain and are critical for establishing high-acuity vision. Eye-specific connections and topographic maps are reiterated multiple times in the brain, initially through the direct projections of retinal ganglion cells (RGCs) to the dorsal thalamus and midbrain, and subsequently through higher-order projections to and from the neocortex. Retinotopic maps are organized such that the spatial arrangement of the neurons of origin is reflected in the order of their axon terminations, and thereby, neighboring neurons project their axons to neighboring parts of the target to form a continuous map.

The developmental mechanisms that generate eye-specific connections and retinotopic maps have been studied intensively, and to date the findings have emphasized roles for distinct types of mechanisms. Eye-specific connections require that RGC axons make a critical pathfinding decision at a midline choice point, resulting in the formation of the optic chiasm and the proper sorting of RGC axons to the left and right sides of the brain (Mason and Sretavan, 1997). Once the RGC axons reach their targets, axons from the two eyes initially overlap, but gradually segregate into eye-specific domains or layers (Godement et al., 1984). Numerous studies have established that neural activity plays a pivotal role in the developmental segregation of RGC axons and higher-order visual projections into eye-specific patterns (Wiesel, 1982; Feller, 2002). Recent studies have shown that the absence of retinal activity prevents the formation of eye-specific layers (Penn et al., 1998; Rossi et al., 2001; Huberman et al., 2002; Stellwagen and Shatz, 2002). However, controversy does exist over whether or not correlated patterned activity that distinguishes RGC axons from the two eyes is the dominant regulator of eye-specific segregation of axons within the visual system. Increasing (Stellwagen and Shatz, 2002) or decreasing (Penn et al., 1998) spontaneous activity in one retina relative to the other alters the normal pattern of innervation, indicating that a competitive process is involved and that perhaps the spiking frequency of RGCs is critical to eye-specific segregation of their axons within the dorsal lateral geniculate nucleus (dLGN). However, Huberman et al. (2003) report that spontaneous RGC activity in general, rather than activity patterns correlated between RGCs within an eye, is a dominant parameter in eye-specific segregation. In addition, intraocular injections of TTX do not fully arrest layer formation in the dLGN (Cook et al., 1999), which implies that mechanisms in addition to action potentials may be involved in segregation. In a higher-order visual projection, Crowley and Katz (1999, 2000) suggest that molecular tags may be key parameters controlling the segregation of geniculocortical axons into eye-specific columns within the primary visual area, although again this is a contested issue (Crair et al., 2001).

The projection from the retina to its major midbrain target, the superior colliculus (SC) of mammals, or its nonmammalian homolog, the optic tectum (OT), has

*Correspondence: mfeller@ucsd.edu (M.B.F.), doleary@salk.edu (D.D.M.O.)
[3]These authors contributed equally to this work.

been the predominant model system for development of topographic axonal connections. The developing retinotectal projections in chicks and rodents early on lack any significant degree of topographic order and exhibit similar mechanisms to generate a refined map, distinct from those in fish and amphibians (McLaughlin et al., 2003a). Initially, in chicks and rodents, RGC axons substantially overshoot their appropriate termination zones (TZs) along the anterior-posterior (A-P) axis of the OT/SC. RGC axons from a given dorsal-ventral (D-V) location also have a broad distribution along the lateral-medial (L-M) tectal axis with a peak in axon density centered around the L-M location of the future TZ (Nakamura and O'Leary, 1989; Simon and O'Leary, 1992a, 1992b, 1992c; Hindges et al., 2002). In rodents, these two features result in RGC axons originating from a small focal source in the retina covering most of the SC at perinatal ages. Topographically appropriate connections are established exclusively by branches that form interstitially along the axon shaft with a bias for the A-P location of their future TZ (Simon and O'Leary, 1992a; Yates et al., 2001) and preferentially extend across the L-M axis toward it (Nakamura and O'Leary, 1989; Hindges et al., 2002; McLaughlin et al., 2003b). Refined topography develops over the first postnatal week through the preferential arborization of appropriately positioned branches and, perhaps more importantly, the large-scale elimination of ectopic branches and arbors and the posterior portions of RGC axons that overshoot their TZ (Nakamura and O'Leary, 1989; Simon and O'Leary, 1992a, 1992b; Yates et al., 2001).

In contrast to the emphasis of neural activity in the development of eye-specific connections, the establishment of retinotopic maps has focused more on the roles of graded axon guidance molecules within the retina and its central targets. Recent studies have defined requirements for EphA receptors and ephrin-A ligands in mapping the temporal-nasal (T-N) axis of the retina along the A-P axis of the OT/SC and EphB receptors and ephrin-B ligands in mapping the D-V axis of the retina along the L-M axis of the OT/SC (McLaughlin et al., 2003a).

During development, a coarse topographic projection is initially formed and then undergoes a large-scale remodeling into a refined map over a period of a few days (McLaughlin et al., 2003a). By extrapolation from the development of eye-specific connections, it has often been postulated that similar activity-dependent mechanisms drive the refinement of topographic maps. However, only a handful of studies have actually addressed the role of neural activity in map refinement; these studies have relied predominantly on pharmacological blockade of retinally mediated activity in RGCs or in the target. In species in which the retinotopic map develops by the direct topographic targeting of RGC axons and their terminal arborization, such as amphibians and fish, pharmacological activity blockade typically has been reported to have little effect on the establishment of topography (Harris, 1980, 1984; Stuermer et al., 1990; O'Rourke et al., 1994; but see Schmidt et al., 2000; Gnuegge et al., 2001). However, zebrafish *macho* mutants, which lack action potentials in RGCs, do have enlarged TZs (Gnuegge et al., 2001). This latter study indicates that activity per se is required to generate precise retinotopy in fish, but does not reveal the relative importance of correlated versus uncorrelated RGC activity.

A Hebbian-like, activity-based mechanism that has been hypothesized to drive retinotopic refinement requires that the firing of neighboring RGCs is strongly correlated and that the correlation in firing declines in a distance-dependent manner; correlated RGC inputs are stabilized and noncorrelated RGC inputs are eliminated (Hebb, 1949; Stent, 1973; Butts, 2002; Debski and Cline, 2002). Interestingly, though, much of the map remodeling in rodents during the first postnatal week occurs before photoreceptors are generated and synaptic circuits connect them to RGCs, and the remodeling process is essentially complete before the onset of visually evoked activity (Wong, 1999; Tian and Copenhagen, 2003). However, during the first postnatal week in mice, spontaneous waves of action potentials propagate across the retina and strongly correlate firing between neighboring RGCs (Galli and Maffei, 1988; Meister et al., 1991; Wong et al., 1993; Wong, 1999). The roles of spontaneous correlated activity in the development of retinotopic maps have not been experimentally tested in any species.

Here we directly test the requirement of retinal waves and correlated RGC activity in map remodeling using mice deficient for the β2 subunit of the neuronal nicotinic acetylcholine receptor (nAChR) ($\beta2^{-/-}$ mice) (Xu et al., 1999). During the first postnatal week, retinal waves are mediated by a network of cholinergic amacrine cells and RGCs (Feller, 2002). $\beta2^{-/-}$ mice lack retinal waves during the first postnatal week (Bansal et al., 2000), coincident with the large-scale remodeling of the initially coarse retinocollicular projection into a topographically refined map (Simon and O'Leary, 1992a; Hindges et al., 2002). We show that even though $\beta2^{-/-}$ mice lack coordinated waves of activity, the majority of individual RGCs are active and exhibit a dramatically diminished neighbor correlation in activity patterns. Despite this maintained activity in RGCs, axons from neighboring RGCs fail to form topographically appropriate TZs characterized by dense overlapping arbors, but instead develop a diffuse network of arbors covering an aberrantly broad expanse of the SC. Although retinal waves mediated by an ionotropic glutamate receptor-based circuit appear at postnatal day 8 (P8) in $\beta2^{-/-}$ mice (Bansal et al., 2000) and visually evoked patterned activity (Rossi et al., 2001) emerges a few days later, the retinocollicular projection fails to develop a refined topographic map. These findings demonstrate that the large-scale remodeling of the mammalian retinocollicular projection that leads to the development of a refined topographic map requires correlated RGC activity during an early brief critical period covering the first postnatal week.

Results

Mice Lacking the β2 Subunit of nAChR Have Uncorrelated RGC Activity

Mice lacking the β2 subunit of the nAChR (Xu et al., 1999) lack nAChR-mediated retinal waves between P1 and P7, as assayed by fluorescence imaging of calcium indicators (Bansal et al., 2000). These previous calcium

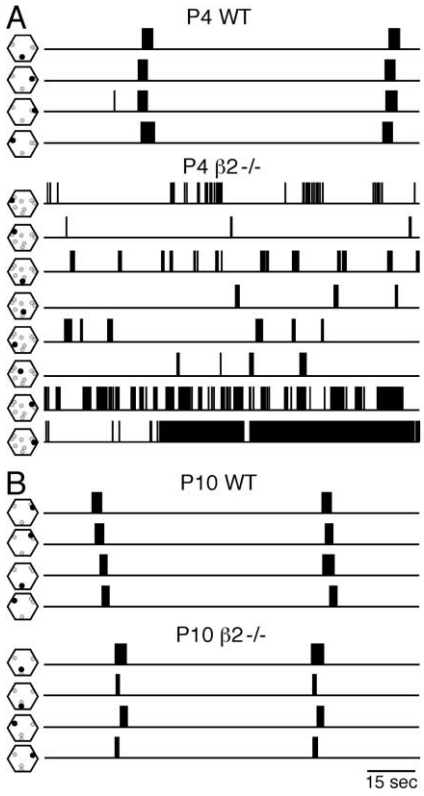

Figure 1. $\beta2^{-/-}$ Retinas Have Altered Firing Patterns during the First Postnatal Week

(A) Spike trains recorded with a multielectrode array (MEA) from four representative neurons in a P4 wt retina and eight representative neurons in a P4 $\beta2^{-/-}$ retina. Note the varied activity patterns and a lack of significant correlation between neurons in the $\beta2^{-/-}$ retina compared to the wt retina.

(B) Spike trains recorded with an MEA from four representative neurons in a P10 wt retina and in a P10 $\beta2^{-/-}$ retina. Note that the activity patterns are similar between neurons and are well correlated in both wt and $\beta2^{-/-}$ retinas. Hexagons to the left of each spike train show the position of the electrode on which that unit was recorded (black circle) relative to the other represented units (gray circles). The maximum extent of the array is 480 μm.

imaging experiments analyzed the patterns of spontaneous activity over large areas (hundreds of square microns) and long time scales (seconds). To determine whether individual retinal neurons in $\beta2^{-/-}$ mice have maintained firing in the absence of waves, we used a multielectrode array (MEA) to record spontaneous action potentials (APs) from wild-type (wt) and $\beta2^{-/-}$ mice. At P4 and P10, wt retinal neurons fire short bursts of APs that are correlated across retinal neurons (Figure 1; see also Supplemental Movies S1 and S3 at http://www.neuron.org/cgi/content/full/40/6/1147/DC1) and fire very few APs between bursts. Similar activity patterns have been reported in neonatal ferrets (Meister et al., 1991; Wong et al., 1993) and mice (Demas et al., 2003). In contrast with wt, in P4 $\beta2^{-/-}$ mice, the correlation in firing patterns between neighboring retinal neurons is substantially reduced (Figure 1 and Supplemental Movie S2). Individual retinal neurons still fire in bursts, but the temporal pattern of bursts differs across retinal neurons. A small percentage of $\beta2^{-/-}$ retinal neurons fire tonically. By P10, after waves reappear in $\beta2^{-/-}$ mice (Bansal et al., 2000), the firing patterns are indistinguishable from wt (Figure 1 and Supplemental Movie S4).

The primary model for how retinal waves drive topographic refinement is that they ensure that the firing of nearby RGCs is more correlated than the firing of distant RGCs (Willshaw and von der Malsburg, 1976; Montague et al., 1991; Butts, 2002). We therefore computed the correlation index for all recorded pairs of neurons. The correlation index is the factor by which the firing rate in neuron B relative to each spike in neuron A is increased above chance. At P4–P5, neighboring wt neurons are more strongly correlated than distant ones (Figure 2A). In $\beta2^{-/-}$ retinas, the correlation index is lower than wt at all separation distances. In addition, the correlation index as a function of distance is constant in $\beta2^{-/-}$ mice, indicating that the source of the small correlations between neurons does not distinguish nearby neurons from distant ones. At P10–P11 (Figure 2A), the correlation index in $\beta2^{-/-}$ mice is similar to wt, indicating strong nearest neighbor correlations are restored.

Another feature of retinal waves is the firing rate of the neurons during a burst. During retinal waves, wt neurons attain high firing rates for a short period of time and then are silent for long periods. To determine the firing rate of individual neurons during the period when they are bursting, we calculated the median interspike interval (ISI) for each neuron. The median ISI is much longer in P4–P5 $\beta2^{-/-}$ neurons (213.68 $\pm$ 13.21 ms, n = 91 neurons) than in P4–P5 wt neurons (93.20 $\pm$ 5.75 ms, n = 46 neurons; t test, $p < 0.01$) (Figure 2B, left), implying that during bursts, wt neurons fired APs at a much higher rate than $\beta2^{-/-}$ neurons. In addition, the distribution of median ISIs in P4–P5 wt is narrower than the distribution for P4–P5 $\beta2^{-/-}$, indicating that firing in wt is more stereotyped across neurons. At P10–P11, a small but significant difference is evident in the average ISI between wt (50.31 $\pm$ 3.13 ms, n = 95 neurons) and $\beta2^{-/-}$ (70.29 $\pm$ 4.72 ms, n = 87 neurons; t test, $p < 0.05$). The range of median ISIs in P10–P11 wt neurons and P10–P11 $\beta2^{-/-}$ neurons is similar (Figure 2B, right).

Though the firing patterns in $\beta2^{-/-}$ retinas are different than wt retinas, the overall level of activity of individual neurons is similar. To compare overall activity levels, we computed the average firing rate, which is a measure of the total number of action potentials fired divided by the duration of the recording. The average firing rate is actually higher in P4 $\beta2^{-/-}$ retinal neurons than wt ($\beta2^{-/-}$, 34.10 $\pm$ 3.91 spikes/min, n = 91; wt, 23.65 $\pm$ 1.33 spikes/min, n = 46; t test, $p < 0.05$) (Figure 2C). At P10–P11, no difference is detected between the average firing rate in $\beta2^{-/-}$ (32.85 $\pm$ 4.74 spikes/min, n = 87) and wt neurons (34.65 $\pm$ 2.74 spikes/min, n = 95).

One limitation of the MEA is that it does not detect neurons that are silent. To estimate the percentage of $\beta2^{-/-}$ RGCs that are spontaneously active, we used fluorescence imaging of the calcium indicator fura-2AM as an indirect measure of RGC depolarization (Figure 3). Bath application of fura-2AM reliably labels all neurons in the RGC layer of acutely isolated retinas from P4 wt and $\beta2^{-/-}$ mice (Figures 3A and 3C). In wt, calcium transients have a characteristic time course of a fast decrease in fluorescence associated with the neuron's depolarization followed by a slower recovery (Figure

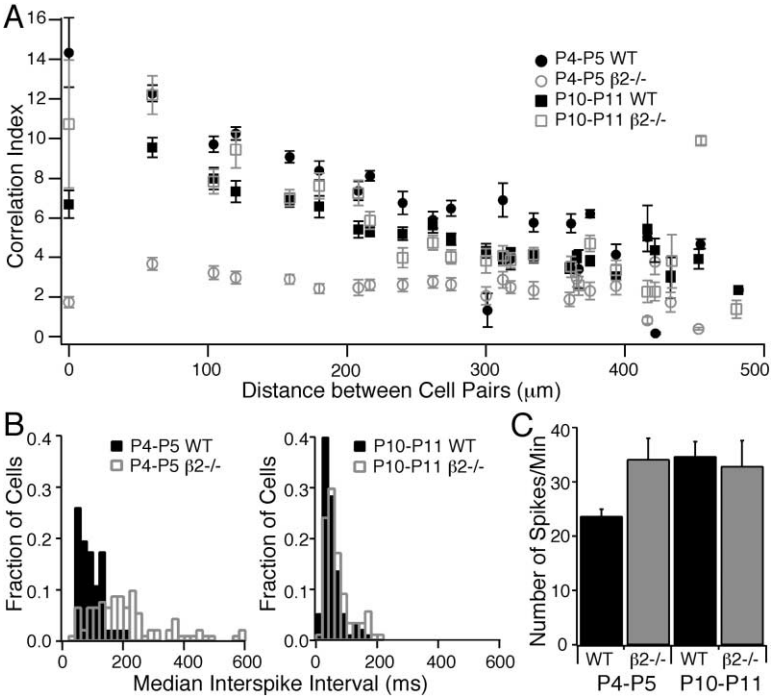

Figure 2. $\beta2^{-/-}$ Neurons Have Increased Firing and Decreased Correlations during the First Postnatal Week but Normal Activity in the Second Week

(A) The correlation index plotted as a function of distance between neuron pairs at P4–P5 and P10–P11 for wt and $\beta2^{-/-}$ mice. The correlation index decreases over distance for neurons at both time points in wt mice and for $\beta2^{-/-}$ mice at P10–P11. However, the correlation index does not vary with distance for P4–P5 $\beta2^{-/-}$ mice, indicating that nearby neurons are no more or less correlated with each other than with distant neurons.

(B) The median interspike interval (ISI) measured at P4–P5 and P10–P11 for both wt and $\beta2^{-/-}$ mice. At P4–P5 there is a broad distribution of median ISI for neurons in $\beta2^{-/-}$ mice, compared to wt mice. However, at P10–P11 the distributions in wt and $\beta2^{-/-}$ mice are indistinguishable.

(C) Summary of the total number of action potentials recorded at P4–P5 and P10–P11 for wt and $\beta2^{-/-}$ mice. At P4–P5 there is a significant increase in the number of spikes per minute in $\beta2^{-/-}$ mice, compared to wt mice. At P10–P11 the distributions of wt and $\beta2^{-/-}$ mice are indistinguishable. Error bars show SEM.

3B). In $\beta2^{-/-}$ retina, the time course of the transients is significantly altered, consistent with the altered temporal structure of bursts of APs recorded with the MEA (Figure 3D).

To distinguish RGCs from displaced amacrine cells (which are estimated to be approximately 40% of the neurons in the mouse RGC layer [Jeon et al., 1998]), we retrogradely labeled RGCs with latex microspheres injected into the contralateral SC of P3 $\beta2^{-/-}$ mice. We computed the fraction of retrogradely labeled neurons at P4 that had spontaneous calcium transients and find that over 60% of the RGCs labeled with microspheres in $\beta2^{-/-}$ mice exhibit calcium transients (Figures 3E and 3F) (62% $\pm$ 10%, n = 70 RGCs, 3 retinas). This percentage is an underestimate since the analysis is sensitive only to changes in intracellular calcium concentrations due to changes in firing rate, thereby excluding tonically firing RGCs. This percentage is higher than that obtained by measuring the fractional change in fluorescence from all neurons in the RGC layer (Figure 3F) (wt, 97% $\pm$ 1%, n = 443 neurons, 4 retinas; $\beta2^{-/-}$, 31% $\pm$ 9%, n = 813 neurons, 8 retinas; t test, $p < 0.01$). Based on these experiments, we estimate that in $\beta2^{-/-}$ mice, more than 60% of RGCs and almost none of the displaced amacrine cells are spontaneously active.

Impaired Topographic Map Refinement in the Developing Retinocollicular Projection in $\beta2^{-/-}$ Mice

In wt mice, topographic organization of the retinocollicular projection gradually develops over the first postnatal week. Figure 4 illustrates the primary features of wt map development that progressively lead to retinotopic organization, revealed in a set of cases with small focal DiI injections of similar size and placement into temporal retina (Simon and O'Leary, 1992a, 1992b; Hindges et al., 2002). At P1, the retinocollicular projection exhibits little evidence of its mature topographic organization. RGC axons extend posteriorly across the SC well beyond their future TZ in anterior SC and have a broad distribution that covers much of the L-M SC axis, with a peak in axon density centered around the L-M location of the future TZ (Figure 4A; Simon and O'Leary, 1992a, 1992b, 1992c; Hindges et al., 2002). Branches extend from RGC axon shafts and their distribution has a modest topographic bias along the A-P axis for their future TZ. At P4, branches near the site of the future TZ exhibit a preferential arborization and the initial axon overshoot is substantially diminished. These complementary processes result in a domain of increased branching and arborization centered on, but much larger than, the appropriate TZ (Figure 4B). At P8, a focal, densely labeled TZ is evident at the correct location, and essentially all ectopic branches and arbors, as well as the posterior portions of the initially overshooting axons, have been eliminated (Figure 4C). Thus, topographic order in the mouse retinocollicular projection develops principally over the first postnatal week and involves both a progressive increase in topographic branching and arborization as well as a large-scale remodeling of the initially diffuse projection.

These findings indicate that the refinement of the retinotopic map in the SC is coincident with the time during which propagation of nAChR-mediated spontaneous retinal waves are observed. To assess the requirement of the nAChR-mediated retinal waves in retinotopic map refinement, we analyzed the topographic organization of the retinocollicular projection in $\beta2^{-/-}$ mice at P7 to P9, by which stage the retinotopic map in wt mice resembles its mature form. We also analyzed the basic pathfinding of RGC axons and the structure and lamination of the SC. Both appear normal in $\beta2^{-/-}$ mice (data

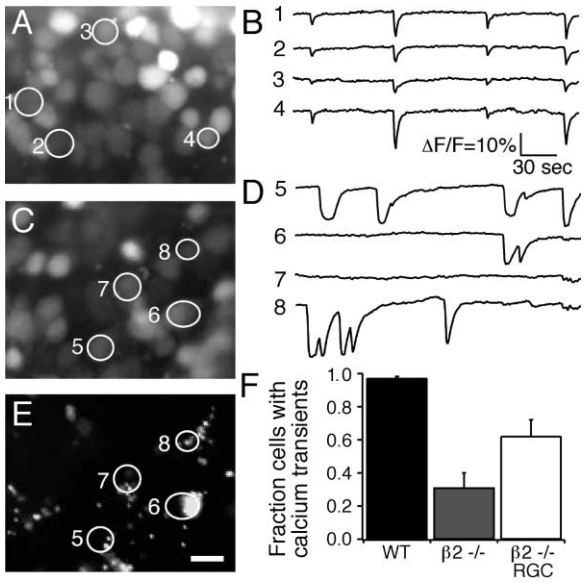

Figure 3. Spontaneous Ca^{2+} Transients in $\beta2^{-/-}$ and Wild-Type Retinas

(A) Fluorescence image of a wt RGC layer loaded with fura-2AM.
(B) Time course of the ΔF/F for each of the numbered, circled cells in (A). In wt retinas, calcium transients occur periodically and are correlated between cells.
(C) Fluorescence images of a $\beta2^{-/-}$ RGC layer loaded with fura-2AM.
(D) Traces of the ΔF/F for each of the numbered, circled cells in (C). In $\beta2^{-/-}$ retinas, calcium transients are not substantially correlated between cells and are of variable durations and intervals.
(E) The same retina as that imaged in (C) imaged with rhodamine optics to visualize fluorescent latex microspheres retrogradely transported from the SC. Cells containing microspheres are RGCs, cells that do not contain microspheres may or may not be RGCs.
(F) Summary of the fraction of cells that have calcium transients for all cells in the RGC layer in wt retinas (black), $\beta2^{-/-}$ retinas (gray), and RGCs retrogradely labeled with microspheres in $\beta2^{-/-}$ retinas (white). Error bars show SD. Scale bar equals 25 μm.

not shown), consistent with previous reports (Rossi et al., 2001). RGC density is also normal in the $\beta2^{-/-}$ mice at P8 (Bansal et al., 2000).

In addition, we analyzed early (P1) and mid (P4) stages of development of the retinocollicular projection in $\beta2^{-/-}$ mice and their wt littermates by making small focal injections of DiI into temporal retina, similar in size and placement to those in the cases illustrated in Figure 4. At both stages, the basic features of retinocollicular map development in $\beta2^{-/-}$ mice resemble those in wt. In P1 $\beta2^{-/-}$ mice (n = 6), RGC axons overshoot their TZ along the A-P axis and have a broad distribution along the L-M axis with a peak centered at the location of the correct TZ (Figure 5A), as in wt (n = 5). At P4, the retinocollicular projection in $\beta2^{-/-}$ mice (n = 5; Figure 5B) is characterized by branching and arborization in a domain much larger than, but surrounding, the TZ, as in their wt littermates (n = 5; Figure 4B). However, the projection at P4 also appears to be topographically more coarse in $\beta2^{-/-}$ mice (Figure 5B) than in their wt littermates (Figure 4B). This finding suggests that map remodeling is impaired $\beta2^{-/-}$ mice as early as P4.

To assess map refinement in $\beta2^{-/-}$ mice, we focused on P8 mice, when the retinotopic map is normally refined, by making a small injection of DiI into temporal retina similar to those used in the cases illustrated in Figure 4C. In wt mice, these injections revealed in every case a small, focal, densely labeled TZ at the appropriate topographic position (n = 10; Figures 4C and 6A). In contrast, in $\beta2^{-/-}$ mice, a small, focal, densely labeled TZ is not observed in any of the cases analyzed (n = 14). Instead, in every $\beta2^{-/-}$ case, an injection of DiI of a similar size to that in the wt cases reveals a "TZ" characterized by a loose array of arborizations spread in a fairly uniform density over an abnormally broad extent of the A-P and L-M axes of the SC (Figures 6B and 6C). Although the TZs observed in the $\beta2^{-/-}$ mice are large and diffuse, injections made at different D-V positions in temporal retina result in a topographically appropriate shift in the diffuse TZ along the L-M SC axis (Figure 6C), indicating a coarse D-V topography.

Although our findings show that the $\beta2^{-/-}$ mice have a significant impairment in map remodeling, one aspect of remodeling does occur to a substantial degree: in the $\beta2^{-/-}$ mice, a sizable proportion of the initially overshooting axons are eliminated from posterior SC as in wt mice. Qualitatively, the diffuse topographic organization of the retinocollicular projection in the $\beta2^{-/-}$ mice roughly resembles the midphase of wt map development wherein arbors are biased for topographic positions but are more broadly distributed (compare Figures 6B and 6C to Figure 4B).

To compare quantitatively the sizes of the retinal injections and the TZs observed in wt and $\beta2^{-/-}$ mice at P7–P9, we measured the percentage of the retina covered by the injection site and used a "signal threshold" analysis to determine the area of the SC that contained fluorescence labeling (see Experimental Procedures; Figure 7A). Since the signal threshold analysis excludes unlabeled space between DiI-labeled arbors within the SC, these data are an underestimate of the increase in coverage of the SC by the expanded TZs observed in the $\beta2^{-/-}$ mice. For P7–P9 wt mice (n = 8), the average retinal DiI injection covered 0.9% ± 0.2% of the surface area of the retina and resulted in a densely labeled TZ occupying an average of 1.4% ± 0.2% of the surface area of the SC (Figure 7A). For $\beta2^{-/-}$ mice at P7–P9 (n = 6), the average injection covered 1.1% ± 0.3% of the retina and resulted in labeling covering 13.8% ± 1.7% of the SC (Figure 7A), about an 8-fold increase in coverage compared to wt (corrected for the slight differences in mean injection sizes). In addition, the two sets of cases are entirely distinct, with no overlap between individual wt and $\beta2^{-/-}$ cases in TZ size for the range of injection sizes used. These data show that although the retinal injection sites for wt versus $\beta2^{-/-}$ mice are indistinguishable in size ($p = 0.6$, Student's unpaired t test), the resulting TZs are significantly larger in $\beta2^{-/-}$ mice ($p < 0.01$). These findings show that the development of dense overlapping clusters of arbors from neighboring RGCs that characterize a TZ in wt mice requires nAChR-mediated correlated retinal activity during the first postnatal week.

To complement the signal-threshold analysis, and to assess whether remodeling along the A-P and L-M axes may be differentially affected, we carried out two additional analyses of TZ coverage in wt and $\beta2^{-/-}$ mice (see Experimental Procedures for details). One analysis,

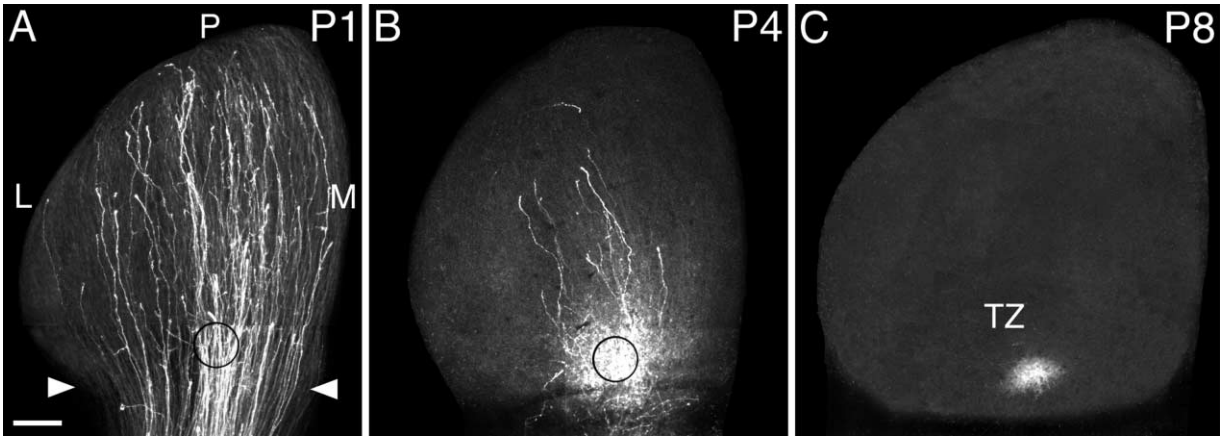

Figure 4. Normal Development of the Topographic Retinocollicular Map Requires Large-Scale Remodeling

Focal injection of the fluorescent lipophilic tracer DiI into temporal retina of wt mice labels RGC axons from a single retinal location. Shown are fluorescence images of DiI-labeled RGC axons in wt SC at the ages indicated.

(A) At P1 RGC axons are dispersed across the entire lateral-medial (L-M) and anterior (arrowheads)-posterior (P) axes of the SC. Essentially all RGC axons extend well posterior to the location of their future TZ (circle). Branches form de novo from the axon shaft in a distribution biased for the A-P location of the future TZ. In addition, branches are directed toward their future TZ along the L-M axis.

(B) At P4 RGC axons with branches near the future TZ preferentially elaborate arbors. Note that many RGC axons have eliminated their initial posterior overshoot.

(C) At P8, a dense focal TZ is labeled at the topographically appropriate location in the SC. The initial axon overshoot is eliminated and no arbors persist outside the TZ. At P8 the retinocollicular map resembles its mature form. Scale bar equals 250 μm.

using the ellipse fitting function of NIH Image software, indicates that the A-P and L-M extents of substantial arborizations are significantly greater in $\beta2^{-/-}$ mice than in wt mice ($p < 0.01$ for each axis). Using another analysis, we confirm that both the A-P and L-M extents of substantial arborizations are significantly greater in $\beta2^{-/-}$ mice than in wt mice: in wt mice, the TZ covers a slightly smaller percentage of the A-P axis of the SC than of the L-M axis (A-P coverage of TZ, 11.3% ± 0.8%; L-M coverage of TZ, 16.1% ± 1.1%; $p < 0.01$); in $\beta2^{-/-}$ mice, the loose array of arbors that form the expanded TZ covers a similar percentage of each axis (A-P axis, 56% ± 2.9%; L-M axis, 51.3% ± 3.5%; $p = 0.32$). Thus, the defective map remodeling in $\beta2^{-/-}$ mice affects both axes to a substantial degree. This latter analysis also shows that the TZ in $\beta2^{-/-}$ mice is about 13-fold larger than in wt. In summary, three independent measures of "TZ" size corroborate one another and confirm that the large-scale remodeling of the initially coarse retinocollicular map in wt mice requires nAChR-mediated correlated retinal activity.

Map Refinement Exhibits an Early Critical Period Coincident with the Phase of nAChR-Mediated Retinal Waves

An important issue is whether the action of correlated activity in generating a refined retinotopic map is limited to a critical period of early postnatal development. The circuit that mediates retinal waves changes during normal postnatal development. During the first postnatal week, spontaneous retinal waves are mediated by activation of nAChRs. At P10, activation of nAChRs is no

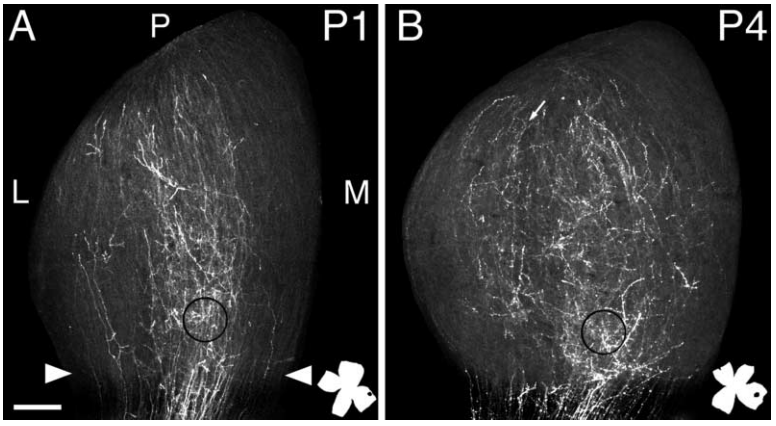

Figure 5. Early Development of the Retinocollicular Projection in $\beta2^{-/-}$ Mice

Focal injection of DiI into temporal retina of $\beta2^{-/-}$ mice labels RGC axons from a single retinal location. Shown are fluorescence images of DiI-labeled RGC axons in $\beta2^{-/-}$ SC at the ages indicated.

(A) At P1, RGC axons are dispersed across the entire lateral-medial (L-M) and anterior (arrowheads)-posterior (P) axes of the SC as in wt. Essentially all RGC axons extend well posterior to the location of their future TZ (circle), as in wt. Branches extend from the axon shaft in a distribution slightly biased for the topographically correct A-P location.

(B) At P4, few RGC axons have eliminated their posterior overshoot in $\beta2^{-/-}$ mice. In addition, branches that form at a relatively low rate in mid-SC and posterior SC have not been eliminated (arrow), as they are in wt mice, resulting in a widespread projection covering much of the SC. The inset in each panel is a tracing of the flat-mounted retina and injection site (black spot) for each case. Temporal is to the right and dorsal is to the top for each retinal tracing. Scale bar equals 250 μm.

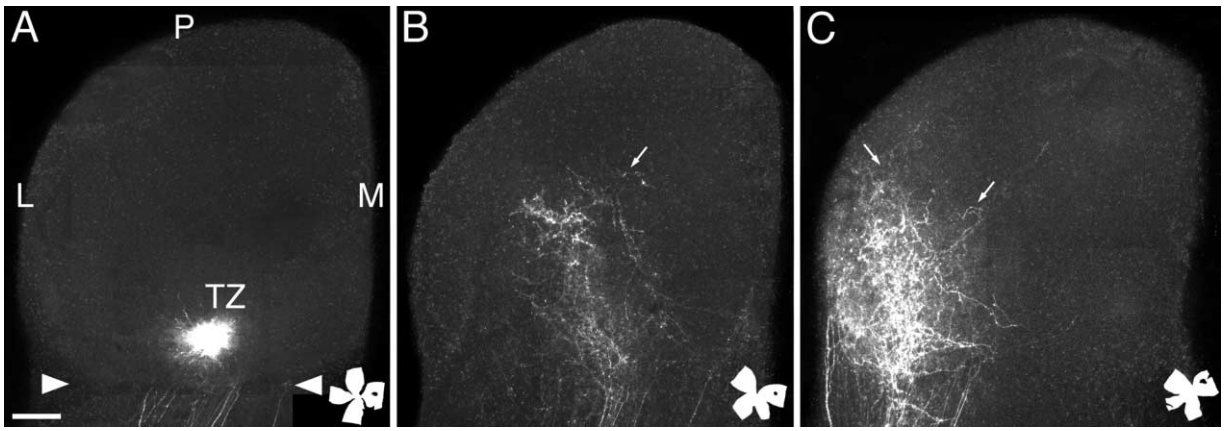

Figure 6. $\beta2^{-/-}$ Mice Have Defective Topographic Remodeling of the Retinocollicular Projection

Fluorescence images of DiI-labeled RGC axons in SC of P8 wt (A) and $\beta2^{-/-}$ (B and C) mice.

(A) Focal injection of DiI into temporal retina of a P7 wt mouse reveals a single, densely labeled TZ in anterior (arrowheads) SC at P8 characteristic of refined topographic organization of the mature retinocollicular projection.

(B and C) Focal DiI injections, similar in size to that in (A), into temporal retina of P7 $\beta2^{-/-}$ mice reveal at P8, TZs characterized by large domains of loosely organized arborizations. The arborizations surround the appropriate topographic position but have not refined into a single dense cluster characteristic of the TZ of wt mice at this age. Furthermore, many RGC axons persist in mid-SC with elaborate arbors (arrows). The inset in each panel is a tracing of the flat-mounted retina and injection site (black spot) for each case. Temporal is to the right and dorsal is to the top for each retinal tracing. L, lateral; M, medial; P, posterior. Scale bar equals 250 μm.

longer requisite; rather, waves are mediated by activation of ionotropic glutamate receptors (Bansal et al., 2000). Therefore, $\beta2^{-/-}$ mice are an excellent system for addressing whether activity-dependent refinement has a critical period because the nAChR-mediated retinal waves coincident with the normal period of large-scale map remodeling over the first postnatal week are absent, but a distinct set of retinal waves mediated by activation of ionotropic glutamate receptors begins at P8, and patterned visual activity begins near the end of the second postnatal week. As described above, we find that correlated patterns of activity among neighboring RGCs is similar at P10 in $\beta2^{-/-}$ and wt mice, indicating that despite the absence of waves during the first postnatal week, a distance-dependent correlation in spiking patterns mediated by ionotropic glutamate receptors in the $\beta2^{-/-}$ mutants are indistinguishable from wt retinas at P10 (Figures 1 and 2; see Supplemental Movies S3 and S4 at http://www.neuron.org/cgi/content/full/40/6/1147/DC1). In addition, the firing patterns induced during the second postnatal week are very similar to those in the first postnatal week in wt mice (Figure 1; Supplemental Movies S1 and S4).

To address whether the onset of patterned activity at the beginning of the second postnatal week results in a delayed retinotopic remodeling, we analyzed the topographic organization of the retinocollicular projection in $\beta2^{-/-}$ mice at the end of the third postnatal week (P19–P22). Thus, these P19–P22 $\beta2^{-/-}$ mice lacked correlated RGC activity during the first postnatal week when the retinocollicular projection normally refines but did experience correlated RGC activity over the second and third postnatal weeks. We focused our analyses on cases with a small injection of DiI into temporal retina similar to those used in the analyses described above to enable a direct comparison of map organization to that in P7–P9 $\beta2^{-/-}$ mice that never experienced correlated RGC activity and P19–P22 wt mice that experienced both the early nAChR-mediated and the late ionotropic glutamate receptor-mediated correlated activity.

As at P7–P9, in P19–P22 wt mice, every case has a small, focal, densely labeled TZ at the appropriate topographic position ($n = 5$; Figures 8A and 8B). In addition, as at P7–P9, in every P19–P22 $\beta2^{-/-}$ case ($n = 11$), we observe an aberrantly large domain of RGC arborizations surrounding the appropriate topographic position, indicating that many if not all of the ectopic arborizations observed in $\beta2^{-/-}$ mice at P7–P9 are retained at P19–P22 (Figures 8C and 8D). To compare quantitatively the sizes of the retinal injections sites and TZs observed in wt and $\beta2^{-/-}$ mice at P19–P22, we measured the focal retinal DiI injections and used the signal-threshold analysis to determine the overall coverage of fluorescence label in the SC, as described above (also see Experimental Procedures). Retinal DiI injection sites at P19–P22 are similar in size in the retina of wt and $\beta2^{-/-}$ mice (wt, 1.3% ± 0.1% of the retina, $n = 5$; $\beta2^{-/-}$, 1.3% ± 0.2%, $n = 6$; $p = 0.8$), but as at P7–P9, the TZs are significantly larger in $\beta2^{-/-}$ mice than in wt at P19–P22 (about 13-fold larger: wt, 0.9% ± 0.2% of the SC; $\beta2^{-/-}$, 11.9% ± 0.4%; $p << 0.01$) (Figure 7B). Again, as at P7–P9, the two sets of cases are entirely distinct with no overlap between individual wt and $\beta2^{-/-}$ cases in TZ size for the range of injection sizes used. The numerous scattered arborizations that characterize the expanded aberrant TZ observed in $\beta2^{-/-}$ mice appear more dense and focused at P19–P22 than at P7–P9. These observations suggest a subtle refinement of RGC axon arborizations after the first postnatal week, although the decrease in percentage coverage of the TZs between the two age groups is not statistically significant in either wt or $\beta2^{-/-}$ mice (wt, P7–P9 versus P19–P22, $p = 0.16$; $\beta2^{-/-}$, P7–P9 versus P19–P22, $p = 0.31$). The aberrantly expanded domain of ectopic RGC arborizations persists

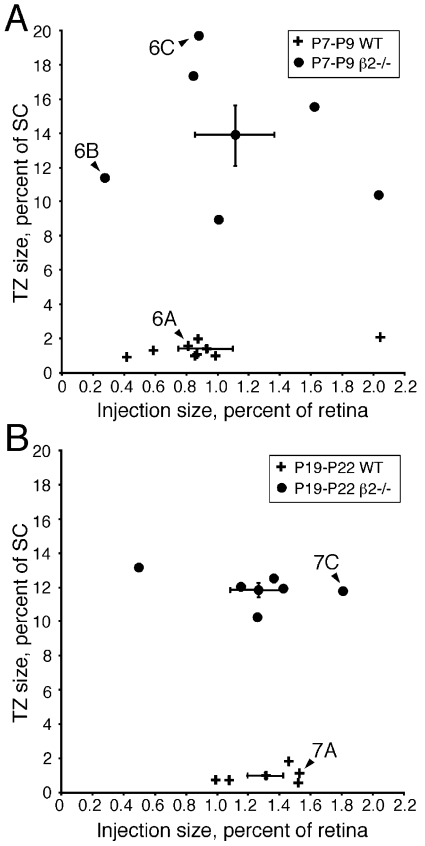

Figure 7. Termination Zones in $\beta2^{-/-}$ Mice Are Significantly Larger than in Wild-Type Mice

Graphs represent the sizes of the retinal DiI injection sites (*x* axis) and percentage of the SC that contains above background fluorescence due to DiI-labeled arborizations (*y* axis) for wt (plus signs) and $\beta2^{-/-}$ (circles) mice at P7–P9 (A) and P19–P22 (B). The average for each data set is represented by the point with error bars (SEM). At both P7–P9 and P19–P22 the injection sizes for wt and $\beta2^{-/-}$ mice are overlapping populations and are not significantly different (see text). However, every TZ observed in $\beta2^{-/-}$ mice is substantially larger than every TZ observed in wt mice at both time points. The cases illustrated in Figures 6 and 8 are indicated.

in $\beta2^{-/-}$ mice greater than 4 months of age (n = 4), whereas wt mice of this age (n = 2) have a small, focal dense TZ (data not shown).

These findings show that $\beta2^{-/-}$ mice retain an aberrantly expanded domain of ectopic RGC arborizations into adulthood that in coverage closely mirrors that observed at the end of the first postnatal week and rule out a developmental delay in the refinement of the retinocollicular projection in $\beta2^{-/-}$ mice. Instead, these findings indicate that large-scale remodeling of the retinocollicular map has a critical period that coincides with the phase of nAChR-mediated spontaneous retinal waves over the first postnatal week.

Discussion

We have used the mouse retinocollicular projection as a model to address the requirements of retinal waves and near neighbor-correlated RGC activity in developing a refined retinotopic map and to determine whether a critical period can be defined for this process. The mammalian retinocollicular projection requires a substantial degree of remodeling to develop a precise retinotopic map. In mice, this remodeling occurs over the first postnatal week and transforms a topographically diffuse projection into a very precise map through the large-scale elimination of overshooting portions of RGC axons that had initially extended well past their correct TZ, as well as the elimination of ectopic branches and arbors. This large-scale remodeling occurs well before the onset of visually evoked activity. However, the remodeling is coincident with a unique phenomenon of spontaneous retinal waves that propagate across the retina in a stochastic manner, generated by a network of cholinergic amacrine cells that interconnect RGCs that express nAChRs. These retinal waves generate correlated patterns of spontaneous activity among neighboring RGCs.

To address whether retinal waves and correlated RGC activity are required for retinotopic map remodeling, we analyzed mice deficient for the β2 subunit of the nAChR, a component required for propagating retinal waves during the first postnatal week. Our findings show that retinal waves and correlated RGC activity are required for retinotopic map remodeling. In addition, our findings demonstrate that the first postnatal week constitutes a critical period during which this remodeling must occur. This mouse model provides significant insight into the respective roles of patterned activity and axon guidance molecules in the development of a topographic map.

$\beta2^{-/-}$ Mice Lack Correlated Patterns of Spontaneous RGC Activity during the First Postnatal Week and Exhibit Defective Map Remodeling

Even though $\beta2^{-/-}$ mice lack retinal waves, we show that retinal neurons, including RGCs, retain a high level of activity in $\beta2^{-/-}$ mice, but correlated activity among neighboring RGCs is substantially diminished. MEA recordings of retinas from wt mice show that retinal neurons spike in a propagating and temporally structured manner and that strong correlations in activity between nearby retinal neurons decreases as a function of distance between them. In contrast, we find that in $\beta2^{-/-}$ retinas, retinal neurons spike in a nonpropagating, temporally disorganized manner. This disorganized spiking in retinal neurons leads to substantially diminished correlations in activity between nearby retinal neurons compared to wt. Unlike in wt retina, then, in $\beta2^{-/-}$ retina, the relative retinotopic positions of RGCs cannot be distinguished on the basis of their spontaneous firing patterns. Therefore, the $\beta2^{-/-}$ mouse is an excellent model to test selectively the role of strong nearest neighbor correlations in patterned RGC activity in the development of a refined retinocollicular topographic map.

The topographic projection of RGC axons to mouse SC is formed in four phases over the first postnatal week: (1) RGC axons enter the SC with a very broad distribution relative to their TZ along the L-M axis and overshoot their TZ along the A-P axis; these features result in RGC axons arising from the same retinal location initially covering much of the surface of the SC; (2) RGC axons branch interstitially along their length with a modest topographic bias for the correct location of

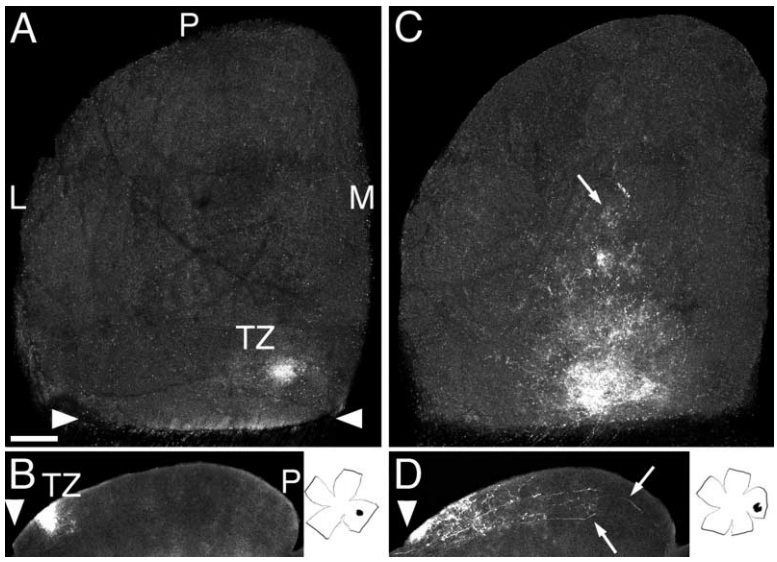

Figure 8. The Retinotopic Map in $\beta2^{-/-}$ Mice Fails to Remodel after Patterned Retinal Activity Resumes, Indicating a Critical Period

Fluorescence images of DiI-labeled RGC axons in SC of P20 wt (A and B) and $\beta2^{-/-}$ (C and D) mice.

(A and B) Focal injection of DiI into temporal retina of a P20 wt mouse reveals a single, densely labeled TZ in anterior (arrowheads) SC.

(B) A 100 μm thick sagittal section through the SC shown in (A); anterior is at the arrowhead, posterior (P) is to the right. A single densely labeled TZ is evident in anterior SC with no axons or branches in mid or posterior SC.

(C and D) Focal DiI injection, similar in size to that shown in (A), into temporal retina of a P20 $\beta2^{-/-}$ mouse. RGC axon arborizations surround the appropriate topographic position but have not refined into a single dense cluster characteristic of the TZ of wt mice at this age. In addition, axons, branches, and arbors are found in aberrant, posterior locations (arrow).

(D) A 100 μm thick sagittal section through the $\beta2^{-/-}$ SC shown in (C). A loose array of arbors is evident in the topographically appropriate anterior SC, although it covers a larger domain than the TZ does in a wt mouse with a similar sized injection at this age. RGC axons, branches, and arbors are also aberrantly found in mid and posterior SC (arrows).

(C and D, insets) Tracing of the flat-mounted retina and injection site (black spot) for each case illustrated. Temporal is to the right and dorsal is to the top of each retina. L, lateral; M, medial. Scale bar equals 250 μm for (A) and (C) and 360 μm for (B) and (D).

their future TZ; (3) these branches arborize in a region surrounding the TZ but considerably larger than its final size; and (4) the initial exuberant projection is remodeled through a large-scale elimination of overshooting axon segments, as well as ectopic branches and arbors, to generate a refined retinotopic map by the end of the first postnatal week (Figure 9).

In contrast to the densely clustered RGC axon arborizations that form the TZ labeled in wt mice at the end of the first postnatal week, in $\beta2^{-/-}$ mice the "TZ" is characterized by a loose array of arborizations spread at a fairly uniform density over an abnormally broad extent of the A-P and L-M axes of the SC (Figure 9). Although these aberrant TZs observed in $\beta2^{-/-}$ mice are large and diffuse, injections made at different D-V positions in temporal retina result in a topographically appropriate shift along the L-M SC axis. Thus, although the topographic map is very diffuse relative to wt mice of a similar age, a coarse topography is evident (Figure 9). This finding indicates that topographic guidance molecules that set up the initial mapping of the D-V axis of the retina along the L-M axis of the SC (for example, the EphB family of receptors and their ephrin-B ligands [Hindges et al., 2002]) function in the absence of patterned retinal activity in $\beta2^{-/-}$ mice. A coarse topography is also evident along the A-P axis in $\beta2^{-/-}$ mice. Although the arborizations of temporal axons cover a much greater extent of the A-P axis in the SC of $\beta2^{-/-}$ mice than in wt at the end of the first postnatal week, they do not cover the entire A-P axis as they do earlier in development in both wt and $\beta2^{-/-}$ mice. This finding indicates that topographic guidance molecules that set up the initial mapping of the T-N axis of the retina along the A-P axis of the SC, for example, the EphA family of receptors and their ephrin-A ligands (Frisen et al., 1998; Feldheim et al., 2000; Brown et al., 2000), also function in the absence of patterned retinal activity in $\beta2^{-/-}$ mice.

Although our findings show that $\beta2^{-/-}$ mice have a significant impairment in map remodeling, some features of retinotopic refinement are relatively intact. In the $\beta2^{-/-}$ mice, the great majority of overshooting axon segments are eliminated from posterior SC, whereas in wt mice, all overshooting RGC axon segments are eliminated. However, the distribution of RGC axons does cover a greater extent of the A-P axis in the mutant, likely due to the establishment and maintenance of ectopic arbors that sustain overshooting components of the axon to the location of the ectopic arbor. Our findings reveal the roles and limitations of axon guidance molecules in retinocollicular map development and show that the map remodeling process depends upon nAChR-mediated correlated RGC activity that drives neighboring RGCs to form tightly clustered axon arborizations in the SC. Taken together, we conclude that graded molecular guidance mechanisms, including Ephs and ephrins, establish an initial coarse topographic order in the retinocollicular projection, and that correlated patterns of spontaneous activity among RGCs are required to remodel the initially diffuse projection into a refined retinotopic map.

We interpret the defective remodeling in the $\beta2^{-/-}$ mice to be due to the lack of early cholinergic retinal waves and correlated spontaneous activity amongst RGCs. However, high-affinity [^{3}H]epibatidine binding implies the existence of β2-containing nAChRs in mouse SC (Marks et al., 2002), suggesting the possibility that the defective map remodeling in $\beta2^{-/-}$ mice may be due in part to a loss of potential nAChR function at retinocollicular synapses. However, such an effect should be minimal, because all RGC axons are glutamatergic. In addition, chronic delivery to the rat SC of dihydro-β-erythroidine, an nAChR antagonist with a high affinity for β2-containing nAChRs and a greater degree of specificity for β2-containing nAChRs than epibati-

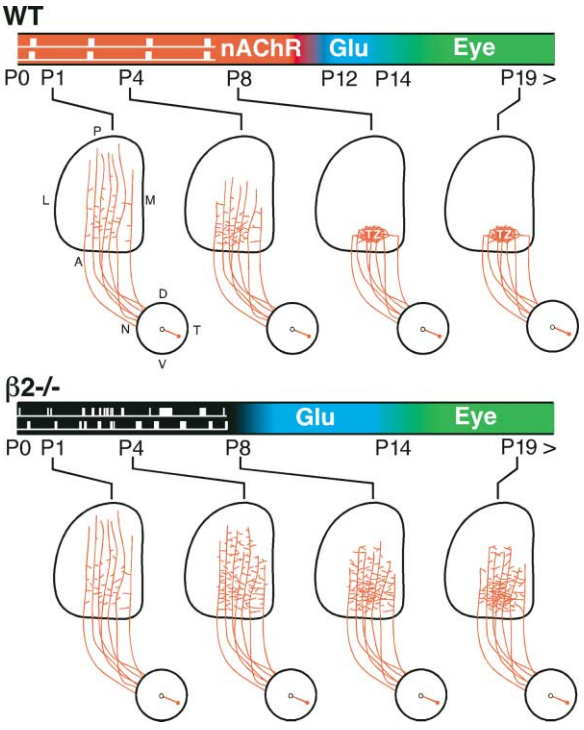

Figure 9. The β2 Subunit of the Neuronal Nicotinic Acetylcholine Receptor Is Required for Spontaneous, Correlated Waves of Retinal Activity and Retinocollicular Map Remodeling during a Brief Critical Period

In wt mice, spontaneous waves of activity, which require the β2 subunit of the nAChR, propagate across the retina until P12 (white spike trains inside red bar; nAChR). During this period, the critical events in topographic map formation occur. Initially, at P1, RGC axons have extended well posterior to their future TZ but form topographically appropriate branches. At P4, the initial RGC axon overshoot has decreased and some branches form arbors in and around the future site of the TZ. By P8, large-scale remodeling of the initially diffuse projection is complete and a refined, dense TZ is evident in the correct topographic position. At P19 the TZ is essentially unchanged from its appearance at P8. At around P12, an ionotropic-glutamate receptor-mediated process (blue, Glu) emerges and is responsible for a second set of retinal waves. In addition, visually evoked activity begins around P10, and the eyes open at the end of the second postnatal week, allowing for patterned visually evoked RGC responses (green, Eye).

In $\beta2^{-/-}$ mice, the nAChR-dependent spontaneous retinal waves are absent; spontaneous RGC activity persists but is not significantly correlated (white spike trains inside black bar). At P1 RGC axons overshoot their TZ, as in wt, and form interstitial branches from the axon shaft. By P4 very little refinement has taken place, most RGC axons have not pruned their initial overshoot, and many branches persist in aberrant locations. In $\beta2^{-/-}$ mice, the ionotropic-glutamate receptor-mediated retinal waves begin at P8. However, at P8 in $\beta2^{-/-}$ mice, the retinotopic map is topographically aberrant: dense TZs have not formed; instead, the TZ is characterized by a large domain of loosely organized arborizations. Substantial topographic remodeling of the retinocollicular map fails to occur by P19–P22 in $\beta2^{-/-}$ mice.

dine, over the entire period of postnatal map remodeling (Simon and O'Leary, 1992a, 1992b, 1992c; Hindges et al., 2002), has no observed effect on retinotopic refinement (Simon et al., 1992). In contrast, the same group showed that the NMDA receptor antagonists, AP5 and MK801, applied in the same manner to the rat SC (Simon et al., 1992), or TTX injected into the rat eye to block all RGC activity (D.K. Simon and D.D.M. O'Leary, 1990, Soc. Neurosci., abstract) result in the abnormal retention of a small proportion of overshooting RGC axons and ectopic branches and arbors. Although these studies were performed in rats, map development in rats is indistinguishable from that in mice (Simon and O'Leary, 1992a, 1992b, 1992c; Hindges et al., 2002; present study). Therefore, we conclude that the defective map remodeling in $\beta2^{-/-}$ mice is due primarily, if not entirely, to the diminished correlation in spiking patterns between neighboring RGCs.

Map Refinement Exhibits an Early Critical Period Coincident with the Phase of nAChR-Mediated Retinal Waves

During the first postnatal week, retinal waves are mediated by a network of cholinergic amacrine cells and are absent in $\beta2^{-/-}$ mice. A distinct form of retinal waves mediated by an ionotropic glutamate receptor-based circuit appear at P8 in $\beta2^{-/-}$ mice, a few days before they are normally seen in wt retina (Bansal et al., 2000). We show here using an MEA that correlated patterns of activity among neighboring RGCs is similar at P10 in $\beta2^{-/-}$ and wt mice, indicating that ionotropic glutamate receptor-mediated correlated activity is intact and of a normal nature in the $\beta2^{-/-}$ mutants. Visually evoked activity emerges by P10 (Tian and Copenhagen, 2003) and is patterned by the end of the second week when the eyelids open. However, our quantitative analyses of the retinocollicular projection in $\beta2^{-/-}$ mice at the end of the third postnatal week and our qualitative analysis of the projection in adult $\beta2^{-/-}$ mice reveal that its topographic organization closely resembles the diffuse projection observed at the end of the first postnatal week and is characterized by an aberrantly broad distribution of ectopic arborizations surrounding, but extending well beyond, the appropriate location for the TZ (Figure 9). Therefore, although these $\beta2^{-/-}$ mice lack correlated RGC activity during the first postnatal week when the retinocollicular projection normally undergoes a large-scale remodeling, they do experience correlated RGC activity over the second postnatal week and beyond yet fail to exhibit any significant map remodeling. These findings demonstrate that the large-scale remodeling of the retinocollicular projection that leads to the development of a refined topographic map requires correlated RGC activity during an early brief critical period limited to the first postnatal week. We conclude, then, that a primary role for the early cholinergic-mediated retinal waves that occur during the first postnatal week in mice is to drive, prior to the onset of visually evoked patterned activity, the correlated activity-dependent development of retinotopic mapping in the SC.

In the absence of nAChR-mediated waves during the first postnatal week, $\beta2^{-/-}$ mice do not form eye-specific layers in the dLGN and, in contrast to wt mice, projections from the two eyes remain overlapped (Rossi et al., 2001; Muir-Robinson et al., 2002). However, after P8, correlated RGC activity due to ionotropic glutamate receptor-mediated waves and visually evoked patterned responses do drive the remodeling of RGC axons from the two eyes into eye-specific patches, although in an

aberrant distribution relative to wt (Muir-Robinson et al., 2002). Thus, the early nAChR-mediated waves are required to drive normal eye-specific layering of retinogeniculate projections, but the later correlated activity patterns are sufficient to drive the competitive interactions that lead to eye-specific segregation (Muir-Robinson et al., 2002; Ruthazer et al., 2003). These findings differ from ours in that topographic map remodeling in the retinocollicular projection fails to occur in the $\beta2^{-/-}$ mice even after the onset of correlated patterns of RGC activity at the beginning of the second postnatal week.

Relationship to Previous Studies of the Role of Activity in Retinotopic Map Refinement

A handful of previous studies used pharmacological blockade of neural activity to address its role in retinotopic map refinement during development in newts/axolotls (Harris, 1980, 1984), zebrafish (Stuermer et al., 1990), and frog (O'Rourke et al., 1994) but found no significant changes in the organization of the retinotopic map. In contrast, Gnuegge et al. (2001) used a zebrafish mutant, *macho*, which exhibits a downregulation of functional voltage-gated sodium channels in RGCs beginning at 5 days postfertilization (dpf), resulting in RGCs lacking action potentials. Analysis of *macho* reveals enlarged RGC arbors in the tectum at 6 dpf but not earlier. Consistent with this result, in wt zebrafish treated with TTX between 2 and 4 dpf and analyzed 2 days later, enlarged arbors as observed in *macho* are seen at 6 dpf but not 4 dpf (Gnuegge et al., 2001). In addition, Schmidt et al. (2000) have reported that MK801, but not AP5, treatment of zebrafish to block NMDA receptors during development results in enlarged retinal arbors in the tectum. Their findings suggest that NMDA blockade in tectum randomizes the elimination of branches but does not affect their formation, resulting in enlarged arbors. Although these analyses do not test the role of correlated RGC activity, the authors conclude that RGC activity is necessary for stabilization of the retinotopic map in zebrafish tectum. Analysis of a mouse deficient in calcium-stimulated adenylate cyclase 1 suggests that this process of map stabilization involves an activity-dependent modulation of a cAMP signaling cascade (Ravary et al., 2003).

Goldfish reared for 1.5 to 2 years under strobe-light conditions, which synchronizes the firing patterns of RGC axons, also have enlarged retinal arbors in the tectum (Schmidt and Buzzard, 1993). Although this study is consistent with a role for correlated RGC activity in controlling the resolution of the retinotopic map, because of species-specific differences in retinotectal development and remodeling (McLaughlin et al., 2003a) and other issues, it is difficult to relate this result to our findings. For example, it is not clear whether the arbor enlargement is due to reduced arbor refinement or enhanced arbor growth. The latter possibility is plausible since the strobe treatments likely increase overall RGC firing, and increased activity increases BDNF expression in the visual system (see Discussion below), and increased BDNF produces enlarged arbors (Cohen-Cory and Fraser, 1995; Cohen-Cory, 1999; Alsina et al., 2001). In addition, given the lengthy period of the strobe treatment, it is not clear whether this is a study of developmental mechanisms or later plasticity. Others have suggested that the mechanisms for development of patterned visual projections may be distinct from those that mediate plasticity in these projections later in life (Crair et al., 2001).

A recent retrograde labeling study suggests that long-term blockade (6 weeks) of multiple receptor types, including nAChRs, locally in mature frog tectum destabilizes the refined retinotopic map and generates a more coarse RGC projection (Yu et al., 2003), presumably by inhibiting release of glutamate at retinotectal synapses (Edwards and Cline, 1999; Butt et al., 2000). Although this is a distinct phenomenon from that of developmental map remodeling that we are studying, this finding indicates a role for activity in maintaining a stable retinotopic map throughout the life of animals such as frogs that, because of disparate continued growth of the retina and tectum, require constant remodeling of the retinotectal projection.

The early retinotectal projection in chicks and rats is substantially more topographically diffuse than in amphibians and fish. In both chick and rat, pharmacological activity blockade prevents the elimination of only a very small proportion of overshooting RGC axon segments and aberrant branches and arbors (Kobayashi et al., 1990; Simon et al., 1992). Even under these activity blockades, a normal appearing, dense TZ forms at the topographically correct location over the same time frame as in untreated animals, and the elimination of the great majority of overshooting RGC axons and ectopic arbors also occurs.

Among the important distinctions between our studies using the $\beta2^{-/-}$ mouse and all previous studies that have addressed the role of activity in retinotopic map refinement is that previous studies either blocked all RGC activity or blocked synaptic transmission between the retina and OT/SC. Therefore, these studies did not test the requirement for correlated action potentials among neighboring RGCs induced by retinal waves. In addition, these other studies have the added potential for secondary consequences on the visual system due to the method of drug delivery and uncertainties about the completeness of the activity blockade and specificities of the pharmacological reagents. Further, neural activity is also known to regulate gene expression and neural maturation, as well as maintaining cell homeostasis; therefore, the types of activity blockade used in previous studies of map remodeling could have nonspecific effects on these features. For example, recent studies suggest that a proper rate of growth by RGC axons requires spontaneous electrical activity that resembles physiological levels (Goldberg et al., 2002). In addition, neural activity and cAMP elevation in RGCs results in a rapid translocation of the neurotrophin receptor trkB from intracellular stores to the plasma membrane (Meyer-Franke et al., 1998). Neurotrophin expression and release, including BDNF in the visual system, can be enhanced by elevated neural activity and diminished by depressed neural activity (Zafra et al., 1990, 1992; Balkowiec and Katz, 2000; Lein and Shatz, 2000; West et al., 2001; Tao et al., 2002). BDNF and trkB are of particular relevance to retinotopic map refinement since increases or decreases in BDNF in frog tectum enlarge or reduce RGC arbors, respectively (Cohen-Cory and Fraser, 1995;

Cohen-Cory, 1999; Alsina et al., 2001). A recent study has also reported an activity-dependent mRNA splicing that controls the export of NMDA receptor subunits from the endoplasmic reticulum to postsynaptic densities (Mu et al., 2003). This feature is also of particular relevance to retinotopic map development because the NMDA receptor acts as a postsynaptic detector of correlated activity for RGCs (Debski and Cline, 2002; Ruthazer et al., 2003).

Thus, activity blockade can lead to changes in gene expression and protein distribution and release that can have significant effects on neuronal viability, maturation, and axonal connections independent of a direct effect of neural activity per se. Although genetically altered mice are also susceptible to caveats, we show that the majority of RGCs maintain spontaneous spiking during the first postnatal week in $\beta2^{-/-}$ mice at an overall level similar to that in wt retina, and subsequent to that the $\beta2^{-/-}$ mice develop normal ionotropic glutamate receptor-mediated RGC activity patterns. Therefore, caveats related to activity blockade should be minimal in the $\beta2^{-/-}$ mice compared to the previous studies. In addition, many relevant features in the $\beta2^{-/-}$ mice are normal, including RGC density, stratification and distribution of ChAT and VAChT immunopositive cells (Bansal et al., 2000), visual acuity in the retina (Rossi et al., 2001), RGC axon pathfinding, and early development of the retinocollicular projection, as well as histological features of the SC (present study).

Conclusions

Here we have demonstrated that nAChR-mediated retinal waves are required for normal refinement of retinotopic maps during an early critical period. Based on this conclusion, we hypothesize that a crucial feature of axon guidance molecules that govern the development of the initial retinotopic map is to ensure that sufficient RGC connections are made near the topographically correct location to allow correlated patterns of RGC spiking to promote stabilization and colocalization of arbors from neighboring RGCs that results in the large-scale remodeling seen in wt mice. The coarse retinocollicular map that we observe in the $\beta2^{-/-}$ mice is the best that topographic guidance molecules can develop when left to their own devices. However, this proves to be sufficient when partnered with correlated patterned activity during an early postnatal critical period, and together these distinct mechanisms cooperate to generate a refined retinotopic map.

Experimental Procedures

Acute Retina Preparation

Wild-type and $\beta2^{-/-}$ mice (P4–P11) were anesthetized with isofluorane and decapitated. Retinas were isolated in cold (4°C) artificial cerebrospinal fluid (ACSF) containing (in mM): 119 NaCl, 26.2 $NaHCO_3$, 11 glucose, 2.5 KCl, 1.0 KH_2PO_4, 2.5 $CaCl_2$, and 1.3 $MgCl_2$. Retinas were cut into thirds, mounted RGC side up on filter paper, and kept at 32°C in ACSF bubbled with 95% O_2/5% CO_2 until use (1–6 hr). During experiments, preparations were superfused continuously with oxygenated ACSF warmed to 32°C.

Optical Recording

As previously described (Bansal et al., 2000), retinal whole-mounts were incubated with 10 μM fura-2AM (Molecular Probes) (50 μg fura-2AM in 50 μl of 2% (w/v) pluronic acid in DMSO placed into 5 ml ACSF) in an oxygenated chamber at 30°C for 2 hr. Images were acquired with a cooled CCD camera (Orca ER, Hamamatsu) through a 40× water immersion objective (Neofluor, Zeiss) using shuttered 380 nm illumination (DG4, Sutter Instruments) at 1 frame/s with a 300 ms exposure. Regions of interest (ROIs) were defined for the soma of every discernible neuron. RGCs were retrogradely labeled by injection of fluorescent latex microspheres (Lumafluor) into the SC of anesthetized P3 mice. One day (16–24 hr) later, the mice were utilized for optical recording. ROIs were defined for RGCs in the retrogradely labeled retinas via the presence of a cluster of fluorescent latex microspheres. Fractional changes in average fluorescence intensity (ΔF/F) were computed for each ROI and corrected for bleaching.

Multielectrode Array Recordings and Analysis

Retina pieces mounted on filter paper were placed RGC side down onto a flat, 480 μm diameter hexagonal array of 61 extracellular electrodes spaced 60 μm apart. During recording, the retina was continuously perfused with oxygenated ACSF with the bath temperature at 32°C–35°C.

Spike times, peaks, and widths were digitized with a temporal resolution of 0.05 ms (Meister et al., 1994). Spikes were manually segregated into single units by selecting distinct clusters in scatter plots of spike height and width recorded on each electrode (Meister et al., 1994) and verifying the presence of a refractory period in the spike trains from each cluster. Spikes recorded on multiple electrodes were identified by temporal coincidence; only spikes from the electrode with the most clearly defined cluster were further analyzed. Between 10 and 65 unique units were identified from each retina piece. Cells were considered to be at the position of the electrode on which they were recorded.

We computed three measures of the spiking properties of retinal neurons for each single unit recorded. (1) The median interspike interval in a spike train was taken as the average firing rate. (2) The average number of action potentials was calculated by summing the total number of action potentials and dividing by the length of the recording. (3) Correlation index was calculated as described in Wong et al. (1993). Briefly, the number of spikes from neuron A that occurred within ±100 ms of a spike in neuron B divided by the number of spike pairs that would have occurred by random chance.

$$\text{Correlation Index} = \frac{N_{AB(-0.1\ s,\ +0.1\ s)} \cdot T}{N_{A(0,T)} \cdot N_{B(0,T)} \cdot (0.2\ s)}$$

N_{AB} = number of spike pairs from neurons A and B for which neuron B fires within ±100 ms of neuron A; T = the total recording time; $N_{A(0,T)}$ = total number of spikes in neuron A; $N_{B(0,T)}$ = total number of spikes in neuron B.

Since firing rates were often very different between both neurons in a pair, the correlation index was calculated using both N_{AB} and N_{BA}. For statistical analysis (IgorPro, Wavemetrics, Inc.), units from each recorded age (P4–P5 and P10–P11) and condition (wt and $\beta2^{-/-}$) were grouped and unpaired Student's t test were performed.

Anterograde RGC Axon Labeling and Quantification

Anterograde labeling was performed essentially as previously described (Simon and O'Leary, 1992a). A discrete, focal injection of a 10% DiI solution (Molecular Probes) in DMF was made into the retina. One day (14–24 hr) after injection, whole-mounts of the dorsal midbrain, including the SC, were prepared from transcardially perfused animals and imaged prior to knowledge of genotype. Retinas were flat-mounted and examined to confirm that all labeled RGC axons originated from the single injection site. Injection sizes, retina sizes, TZ sizes, and SC sizes were quantified using Adobe Photoshop software to analyze digital images taken with a Zeiss LSM510 confocal microscope or a Retiga EX (QImaging) digital camera. Cases quantified had similar background and DiI labeling efficacy. For injection size quantification, the number of pixels exceeding 5 times the background luminosity value of unlabeled retinal tissue was divided by the total number of pixels representing the entire neural retina and expressed as a percentage. All retinal analyses were performed blind to genotype. TZ sizes were determined similarly using a threshold of 1.5 times (for P7–P9) or 1.2 times (for

P19–P22) the background luminosity of unlabeled SC divided by the number of pixels representing the SC. Pixels that met the luminosity threshold but were clearly not due to DiI (such as autofluorescent debris) were removed prior to analysis. This pixel measurement accounts for space occupied by axons and arbors and does not account for total surface area covered. The extent of TZ expansion along the A-P and L-M axes was measured with two methods. NIH Image ellipse fitting analysis was used for the measurement of the major and minor axes and each measurement assigned to the proper SC axis. For the analysis of the linear extent of the TZs along the A-P and L-M axes, the most lateral, medial, anterior, and posterior pixels on the thresholded images were marked, measured, and compared to the most lateral, medial, anterior, and posterior borders of the SC to obtain a percentage of each axis covered by the TZ. The same thresholded images were used for all analyses reported.

Acknowledgments

This work was supported by NIH grant RO1 EY07025 (D.D.M.O.), grants from the Klingenstein Foundation, McKnight Foundation, Whitehall Foundation, March of Dimes, and NIH (RO1 EY13528) (M.B.F.), and an NSF Graduate Fellowship (C.L.T.). We thank A. Beaudet for the β2 mutant mice and E.J. Chichilnisky for making his MEA available to us.

Received: October 2, 2003
Revised: November 3, 2003
Accepted: November 20, 2003
Published: December 17, 2003

References

Alsina, B., Vu, T., and Cohen-Cory, S. (2001). Visualizing synapse formation in arborizing optic axons in vivo: dynamics and modulation by BDNF. Nat. Neurosci. *4*, 1093–1101.

Balkowiec, A., and Katz, D.M. (2000). Activity-dependent release of endogenous brain-derived neurotrophic factor from primary sensory neurons detected by ELISA in situ. J. Neurosci. *20*, 7417–7423.

Bansal, A., Singer, J.H., Hwang, B., and Feller, M.B. (2000). Mice lacking specific nAChR subunits exhibit dramatically altered spontaneous activity patterns and reveal a limited role for retinal waves in forming ON/OFF circuits in the inner retina. J. Neurosci. *20*, 7672–7681.

Brown, A., Yates, P.A., Burrola, P., Ortuno, D., Vaidya, A., Jessell, T.M., Pfaff, S.L., O'Leary, D.D.M., and Lemke, G. (2000). Topographic mapping from the retina to the midbrain is controlled by relative but not absolute levels of EphA receptor signaling. Cell *102*, 77–88.

Burden, S.J., Berg, D., and O'Leary, D.D.M. (2003). Target selection, topographic maps, and synapse formation. In Fundamentals of Neuroscience, L.R. Squire, F.E. Bloom, S.K. McConnell, J.L. Roberts, N.C. Spitzer, and M.J. Zigmond, eds. (San Diego, CA: Academic Press), pp. 469–498.

Butt, C.M., Pauly, J.R., and Debski, E.A. (2000). Distribution and development of nicotinic acetylcholine receptor subtypes in the optic tectum of *Rana pipiens*. J. Comp. Neurol. *423*, 603–618.

Butts, D.A. (2002). Retinal waves: implications for synaptic learning rules during development. Neuroscientist *8*, 243–253.

Cohen-Cory, S. (1999). BDNF modulates, but does not mediate, activity-dependent branching and remodeling of optic axon arbors in vivo. J. Neurosci. *19*, 9996–10003.

Cohen-Cory, S., and Fraser, S.E. (1995). Effects of brain-derived neurotrophic factor on optic axon branching and remodelling in vivo. Nature *378*, 192–196.

Cook, P.M., Prusky, G., and Ramoa, A.S. (1999). The role of spontaneous retinal activity before eye opening in the maturation of form and function in the retinogeniculate pathway of the ferret. Vis. Neurosci. *16*, 491–501.

Crair, M.C., Horton, J.C., Antonini, A., and Stryker, M.P. (2001). Emergence of ocular dominance columns in cat visual cortex by 2 weeks of age. J. Comp. Neurol. *430*, 235–249.

Crowley, J.C., and Katz, L.C. (1999). Development of ocular dominance columns in the absence of retinal input. Nat. Neurosci. *2*, 1125–1130.

Crowley, J.C., and Katz, L.C. (2000). Early development of ocular dominance columns. Science *290*, 1321–1324.

Demas, J., Eglen, S.J., and Wong, R.O. (2003). Developmental loss of synchronous spontaneous activity in the mouse retina is independent of visual experience. J. Neurosci. *23*, 2851–2860.

Debski, E.A., and Cline, H.T. (2002). Activity-dependent mapping in the retinotectal projection. Curr. Opin. Neurobiol. *12*, 93–99.

Edwards, J.A., and Cline, H.T. (1999). Light-induced calcium influx into retinal axons is regulated by presynaptic nicotinic acetylcholine receptor activity in vivo. J. Neurophysiol. *81*, 895–907.

Feldheim, D.A., Kim, Y.I., Bergemann, A.D., Frisen, J., Barbacid, M., and Flanagan, J.G. (2000). Genetic analysis of ephrin-A2 and ephrin-A5 shows their requirement in multiple aspects of retinocollicular mapping. Neuron *25*, 563–574.

Feller, M.B. (2002). The role of nAChR-mediated spontaneous retinal activity in visual system development. J. Neurobiol. *53*, 556–567.

Frisen, J., Yates, P.A., McLaughlin, T., Friedman, G.C., O'Leary, D.D.M., and Barbacid, M. (1998). Ephrin-A5 (AL-1/RAGS) is essential for proper retinal axon guidance and topographic mapping in the mammalian visual system. Neuron *20*, 235–243.

Galli, L., and Maffei, L. (1988). Spontaneous impulse activity of rat retinal ganglion cells in prenatal life. Science *242*, 90–91.

Gnuegge, L., Schmid, S., and Neuhauss, S.C.F. (2001). Analysis of the activity-deprived zebrafish mutant macho reveals an essential requirement of neuronal activity for the development of a fine-grained visuotopic map. J. Neurosci. *21*, 3542–3548.

Godement, P., Salaun, J., and Imbert, M. (1984). Prenatal and postnatal development of retinogeniculate and retinocollicular projections in the mouse. J. Comp. Neurol. *230*, 552–575.

Goldberg, J.L., Espinosa, J.S., Xu, Y., Davidson, N., Kovacs, G.T., and Barres, B.A. (2002). Retinal ganglion cells do not extend axons by default: promotion by neurotrophic signaling and electrical activity. Neuron *33*, 689–702.

Harris, W.A. (1980). The effects of eliminating impulse activity on the development of the retinotectal projection in salamanders. J. Comp. Neurol. *194*, 303–317.

Harris, W.A. (1984). Axonal pathfinding in the absence of normal pathways and impulse activity. J. Neurosci. *4*, 1153–1162.

Hebb, D.O. (1949). The organization of behavior: a neuropsychological theory (New York: Wiley).

Hindges, R., McLaughlin, T., Genoud, N., Henkemeyer, M., and O'Leary, D.D.M. (2002). EphB forward signaling controls directional branch extension and arborization required for dorsal ventral retinotopic mapping. Neuron *35*, 475–487.

Huberman, A.D., Stellwagen, D., and Chapman, B. (2002). Decoupling eye-specific segregation from lamination in the lateral geniculate nucleus. J. Neurosci. *22*, 9419–9429.

Huberman, A.D., Wang, G.-Y., Liets, L.C., Collins, O.A., Chapman, B., and Chalupa, L.M. (2003). Eye-specific retinogeniculate segregation independent of normal neuronal activity. Science *300*, 994–998.

Jeon, C.J., Strettoi, E., and Masland, R.H. (1998). The major cell populations of the mouse retina. J. Neurosci. *18*, 8936–8946.

Kobayashi, T., Nakamura, H., and Yasuda, M. (1990). Disturbance of refinement of retinotectal projection in chick embryos by tetrodotoxin and grayanotoxin. Brain Res. Dev. Brain Res. *57*, 29–35.

Lein, E.S., and Shatz, C.J. (2000). Rapid regulation of brain-derived neurotrophic factor mRNA within eye-specific circuits during ocular dominance column formation. J. Neurosci. *20*, 1470–1483.

Marks, M.J., Whiteaker, P., Grady, S.R., Picciotto, M.R., McIntosh, J.M., and Collins, A.C. (2002). Characterization of [(125) I]epibatidine binding and nicotinic agonist-mediated (86) Rb(+) efflux in interpeduncular nucleus and inferior colliculus of beta2 null mutant mice. J. Neurochem. *81*, 1102–1115.

Mason, C.A., and Sretavan, D.W. (1997). Glia, neurons, and axon pathfinding during optic chiasm development. Curr. Opin. Neurobiol. *7*, 647–653.

McLaughlin, T., Hindges, R., and O'Leary, D.D.M. (2003a). Regulation of axial patterning of the retina and its topographic mapping in the brain. Curr. Opin. Neurobiol. *13*, 57–69.

McLaughlin, T., Hindges, R., Yates, P.A., and O'Leary, D.D.M. (2003b). Bifunctional action of ephrin-B1 as a repellent and attractant to control bidirectional branch extension in dorsal-ventral retinotopic mapping. Development *130*, 2407–2418.

Meister, M., Wong, R.O., Baylor, D.A., and Shatz, C.J. (1991). Synchronous bursts of action potentials in ganglion cells of the developing mammalian retina. Science *252*, 939–943.

Meister, M., Pine, J., and Baylor, D.A. (1994). Multi-neuronal signals from the retina: acquisition and analysis. J. Neurosci. Methods *51*, 95–106.

Meyer-Franke, A., Wilkinson, G.A., Kruttgen, A., Hu, M., Munro, E., Hanson, M.G., Jr., Reichardt, L.F., and Barres, B.A. (1998). Depolarization and cAMP elevation rapidly recruit TrkB to the plasma membrane of CNS neurons. Neuron *21*, 681–693.

Montague, P.R., Gally, J.A., and Edelman, G.M. (1991). Spatial signaling in the development and function of neural connections. Cereb. Cortex *1*, 199–220.

Mu, Y., Otsuka, T., Horton, A.C., Scott, D.B., and Ehlers, M.D. (2003). Activity-dependent mRNA splicing controls ER export and synaptic delivery of NMDA receptors. Neuron *40*, 581–594.

Muir-Robinson, G., Hwang, B.J., and Feller, M.B. (2002). Retinogeniculate axons undergo eye-specific segregation in the absence of eye-specific layers. J. Neurosci. *22*, 5259–5264.

Nakamura, H., and O'Leary, D.D.M. (1989). Inaccuracies in initial growth and arborization of chick retinotectal axons followed by course corrections and axon remodeling to develop topographic order. J. Neurosci. *9*, 3776–3795.

O'Rourke, N.A., Cline, H.T., and Fraser, S.E. (1994). Rapid remodeling of retinal arbors in the tectum with and without blockade of synaptic transmission. Neuron *12*, 921–934.

Penn, A.A., Riquelme, P.A., Feller, M.B., and Shatz, C.J. (1998). Competition in retinogeniculate patterning driven by spontaneous activity. Science *279*, 2108–2112.

Ravary, A., Muzerelle, A., Herve, D., Pascoli, V., Ba-Charvet, K.N., Girault, J.-A., Welker, E., and Gaspar, P. (2003). Adenylate cyclase 1 as a key actor in the refinement of retinal projection maps. J. Neurosci. *23*, 2228–2238.

Reid, R.C. (2003). Vision. In Fundamentals of Neuroscience, L.R. Squire, F.E. Bloom, S.K. McConnell, J.L. Roberts, N.C. Spitzer, and M.J. Zigmond, eds. (San Diego, CA: Academic Press), pp. 469–498.

Rossi, F.M., Pizzorusso, T., Porciatti, V., Marubio, L.M., Maffei, L., and Changeux, J.P. (2001). Requirement of the nicotinic acetylcholine receptor beta 2 subunit for the anatomical and functional development of the visual system. Proc. Natl. Acad. Sci. USA *98*, 6453–6458.

Ruthazer, E.S., Akerman, C.J., and Cline, H.T. (2003). Control of axon branch dynamics by correlated activity in vivo. Science *301*, 66–70.

Schmidt, J.T., and Buzzard, M. (1993). Activity-driven sharpening of the retinotectal projection in goldfish: development under stroboscopic illumination prevents sharpening. J. Neurobiol. *24*, 384–399.

Schmidt, J.T., Buzzard, M., Borress, R., and Dhillon, S. (2000). MK801 increases retinotectal arbor size in developing zebrafish without affecting kinetics of branch elimination and addition. J. Neurobiol. *42*, 303–314.

Simon, D.K., and O'Leary, D.D.M. (1992a). Development of topographic order in the mammalian retinocollicular projection. J. Neurosci. *12*, 1212–1232.

Simon, D.K., and O'Leary, D.D.M. (1992b). Influence of position along the medial-lateral axis of the superior colliculus on the topographic targeting and survival of retinal axons. Brain Res. Dev. Brain Res. *69*, 167–172.

Simon, D.K., and O'Leary, D.D.M. (1992c). Responses of retinal axons in vivo and in vitro to position-encoding molecules in the embryonic superior colliculus. Neuron *9*, 977–989.

Simon, D.K., Prusky, G.T., O'Leary, D.D.M., and Constantine-Paton, M. (1992). N-methyl-D-aspartate receptor antagonists disrupt the formation of a mammalian neural map. Proc. Natl. Acad. Sci. USA *89*, 10593–10597.

Stellwagen, D., and Shatz, C.J. (2002). An instructive role for retinal waves in the development of retinogeniculate connectivity. Neuron *33*, 357–367.

Stent, G.S. (1973). A physiological mechanism for Hebb's postulate of learning. Proc. Natl. Acad. Sci. USA *70*, 997–1001.

Stuermer, C.A., Rohrer, B., and Munz, H. (1990). Development of the retinotectal projection in zebrafish embryos under TTX-induced neural-impulse blockade. J. Neurosci. *10*, 3615–3626.

Tao, X., West, A.E., Chen, W.G., Corfas, G., and Greenberg, M.E. (2002). A calcium-responsive transcription factor, CaRF, that regulates neuronal activity-dependent expression of BDNF. Neuron *33*, 383–395.

Tian, N., and Copenhagen, D.R. (2003). Visual stimulation is required for refinement of ON and OFF pathways in postnatal retina. Neuron *39*, 85–96.

West, A.E., Chen, W.G., Dalva, M.B., Dolmetsch, R.E., Kornhauser, J.M., Shaywitz, A.J., Takasu, M.A., Tao, X., and Greenberg, M.E. (2001). Calcium regulation of neuronal gene expression. Proc. Natl. Acad. Sci. USA *98*, 11024–11031.

Wiesel, T.N. (1982). Postnatal development of the visual cortex and the influence of environment. Nature *299*, 583–591.

Willshaw, D.J., and von der Malsburg, C. (1976). How patterned neural connections can be set up by self-organization. Proc. R. Soc. Lond. B. Biol. Sci. *194*, 431–445.

Wong, R.O. (1999). Retinal waves and visual system development. Annu. Rev. Neurosci. *22*, 29–47.

Wong, R.O., Meister, M., and Shatz, C.J. (1993). Transient period of correlated bursting activity during development of the mammalian retina. Neuron *11*, 923–938.

Xu, W., Orr-Urtreger, A., Nigro, F., Gelber, S., Sutcliffe, C.B., Armstrong, D., Patrick, J.W., Role, L.W., Beaudet, A.L., and De Biasi, M. (1999). Multiorgan autonomic dysfunction in mice lacking the beta2 and the beta4 subunits of neuronal nicotinic acetylcholine receptors. J. Neurosci. *19*, 9298–9305.

Yates, P.A., Roskies, A.R., McLaughlin, T., and O'Leary, D.D.M. (2001). Topographic specific axon branching controlled by ephrin-As is the critical event in retinotectal map development. J. Neurosci. *21*, 8548–8563.

Yu, C.J., Butt, C.M., and Debski, E.A. (2003). Bidirectional modulation of visual plasticity by cholinergic receptor subtypes in the frog optic tectum. Eur. J. Neurosci. *17*, 1253–1265.

Zafra, F., Hengerer, B., Leibrock, J., Thoenen, H., and Lindholm, D. (1990). Activity dependent regulation of BDNF and NGF mRNAs in the rat hippocampus is mediated by non-NMDA glutamate receptors. EMBO J. *9*, 3545–3550.

Zafra, F., Lindholm, D., Castren, E., Hartikka, J., and Thoenen, H. (1992). Regulation of brain-derived neurotrophic factor and nerve growth factor mRNA in primary cultures of hippocampal neurons and astrocytes. J. Neurosci. *12*, 4793–4799.